This is a preprint, the final version is subject to change, of the American Mineralogist (MSA)
Cite as Authors (Year) Title. American Mineralogist, in press.
DOI: https://doi.org/10.2138/am-2019-6897

Revision 1

Effect of hydration on the single-crystal elasticity of pyrope at high pressure and high temperature conditions: implications for the Earth's upper mantle

DAWEI FAN[1,*], JINGUI XU[1], CHANG LU[2], SERGEY N. TKACHEV[4], BO LI[1,3], ZHILING YE[1,3], SHIJIE HUANG[1,3], VITALI B. PRAKAPENKA[4], WENGE ZHOU[1,*]

[1]Key Laboratory of High-Temperature and High-Pressure Study of the Earth's Interior, Institute of Geochemistry, Chinese Academy of Sciences, Guiyang, Guizhou 550081, China

[2]Department of Geological Sciences, Jackson School of Geosciences, The University of Texas at Austin, Austin, Texas 78712, U.S.A.

[3]University of Chinese Academy of Sciences, Beijing 100049, China

[4]Center for Advanced Radiation Sources, University of Chicago, Chicago, Illinois 60437, U.S.A.

[*]Email: fandawei@vip.gyig.ac.cn; zhouwenge@vip.gyig.ac.cn

ABSTRACT:

The elasticity of single-crystal hydrous pyrope with ~900 ppmw H_2O has been derived from sound velocity and density measurements using *in situ* Brillouin light spectroscopy (BLS) and synchrotron X-ray diffraction (XRD) in the diamond anvil cell (DAC) up to 18.6 GPa at room temperature and up to 700 K at ambient pressure. These experimental results are used to evaluate the effect of hydration on the single-crystal elasticity of pyrope at high pressure and high temperature (*P-T*) conditions to better understand its velocity profiles and anisotropies in the upper mantle. Analysis of the results shows that all of the elastic moduli increase almost linearly with increasing pressure at room temperature, and decrease linearly with increasing temperature at ambient pressure. At ambient conditions, the aggregate adiabatic bulk and shear moduli (K_{S0}, G_0) are 168.6(4) GPa and 92.0(3) GPa,

This is a preprint, the final version is subject to change, of the American Mineralogist (MSA)
Cite as Authors (Year) Title. American Mineralogist, in press.
DOI: https://doi.org/10.2138/am-2019-6897

respectively. Compared to anhydrous pyrope, the presence of ~900 ppmw H_2O in pyrope does not significantly affect its K_{S0} and G_0 within their uncertainties. Using the third-order Eulerian finite-strain equation to model the elasticity data, the pressure derivatives of the bulk $[(\partial K_S/\partial P)_T]$ and shear moduli $[(\partial G/\partial P)_T]$ at 300 K are derived as 4.6(1) and 1.3(1), respectively. Compared to previous BLS results of anhydrous pyrope, an addition of ~900 ppmw H_2O in pyrope slightly increases the $(\partial K_S/\partial P)_T$, but has a negligible effect on the $(\partial G/\partial P)_T$ within their uncertainties. The temperature derivatives of the bulk and shear moduli at ambient pressure are $(\partial K_S/\partial T)_P$=-0.015(1) GPa/K and $(\partial G/\partial T)_P$=-0.008(1) GPa/K, which are similar to those of anhydrous pyrope in previous BLS studies within their uncertainties. Meanwhile, our results also indicate that hydrous pyrope remains almost elastically isotropic at relevant high *P-T* conditions, and may have no significant contribution to seismic anisotropy in the upper mantle. In addition, we evaluated the seismic velocities (V_P and V_S) and the V_P/V_S ratio of hydrous pyrope along the upper mantle geotherm and a cold subducted slabs geotherm. It displays that hydrogen has also no significant effect on the seismic velocities and the V_P/V_S ratio of pyrope at the upper mantle conditions.

Keywords: Hydrous pyrope, Single-crystal elasticity, High pressure and high temperature, Brillouin light scattering, Upper Mantle

This is a preprint, the final version is subject to change, of the American Mineralogist (MSA)
Cite as Authors (Year) Title. American Mineralogist, in press.
DOI: https://doi.org/10.2138/am-2019-6897

INTRODUCTION

Silicate garnet is an important constituent in the Earth's upper mantle and transition zone (e.g. Anderson 1989; Anderson and Bass 1984; Bina 2013; Duffy and Anderson 1989; Fan et al. 2009, 2011, 2015b, 2015c, 2017a; Frost 2008; Ita and Stixrude 1992; McDonough and Sun 1995). Mantle compositional models such as pyrolite and piclogite contain ~15% and ~22% of garnet in the upper mantle, respectively (e.g. Bass and Anderson 1984; Ringwood 1975). The percentage can increase to ~40% or even more in the transition zone because pyroxenes progressively dissolve into garnet with increasing pressure (Li B W et al. 2018), forming majorite-garnet solid solutions (Herzberg and Gasparik 1991; Ringwood 1991). Garnet is also one of the important mineral for eclogite (e.g. Kimura et al. 2013; Liu 1980; Xu et al. 2019), formed by high-pressure metamorphism of basalt or gabbro at subduction zones (Poli and Schmidt 2002; Ringwood 1982). Although most natural garnets are complex solid solutions, the most significant component of mantle garnets is its Mg end-member pyrope ($Mg_3Al_2Si_3O_{12}$) (Rickwood et al. 1968; Sinogeikin and Bass 2002). Therefore, pyrope or pyrope-rich garnet is an important mantle mineral, irrespective of what compositional model of Earth's mantle is assumed (Ringwood 1975; Ita and Stixrude 1992).

In addition, previous studies have revealed that hydrogen could be incorporated into nominally anhydrous minerals (NAMs) as structurally bound hydroxyl defects (e.g. Ingrin and Skogby 2000; Skogby 2006; Smyth 1987). NAMs in the Earth's mantle thus have significant implications for the Earth's deep water cycle (e.g. Bolfan-Casanova et al. 2000; Hirschmann 2006; Hirschmann and Kohlstedt 2012; Smyth and Jacobsen 2006). Water can incorporate in garnets as OH- defects associated with charge balancing or oxidation-reduction reactions, or it may substitute Si in the hydrogarnet substitution (Lu and Keppler 1997; Mookherjee and Karato 2010; Withers et al. 1998). Pyrope is a well-known hydrous-bearing NAMs phase in the upper mantle (e.g. Ackermann et al. 1983; Rossman et al. 1989). Natural

pyrope-rich garnets from ultrahigh-pressure metamorphic rocks and kimberlite xenoliths generally contain tens to hundreds of ppmw H_2O (e.g. Aines and Rossman 1984a, 1984b; Bell and Rossman 1992a, 1992b; Beran and Libowitzky 2006; Li H Y et al. 2018). Moreover, experiments on water solubility in garnets also indicated that pyrope and pyrope-rich garnets could dissolve certain amounts of hydrogen, ranging from a few hundred to ~ 1000 ppmw H_2O (Geiger et al. 1991; Lu and Keppler 1997; Mookherjee and Karato 2010; Withers et al. 1998).

The accurate knowledge about the elastic property of pyrope or pyrope-rich garnet is critical for deducing seismic velocities and density profiles and further constructing reliable mantle mineralogy models (e.g. Bass and Anderson 1984; Bass et al. 2008; Duffy and Anderson 1989; Weidner and Wang 2000). Up to now, numerous equation of state studies of pyrope using XRD technique at high pressure/high temperature have been reported (e.g. Leger et al. 1990; Levien et al. 1979; Sato et al. 1978; Wang et al. 1998; Zhang et al. 1998; Zou et al. 2012a). Additionally, the elastic properties of pyrope at ambient and high pressure/temperature conditions have also been investigated using theoretical calculations (e.g. Li et al. 2011; Hu et al. 2016). Moreover, the adiabatic bulk and shear moduli of polycrystalline pyrope have been reported up to 24 GPa and 1700 K by ultrasonic interferometry technique (e.g. Chantel et al. 2016; Chen et al. 1997, 1999; Gwanmesia et al. 2006, 2007; Sumino and Nishizawa 1978; Suzuki and Anderson 1983; Zou et al. 2012b). On the other hand, BLS is another common technique to measure the elasticity of minerals (e.g. Bass and Zhang 2015; Speziale et al. 2014). It has tremendous advantages in deriving the complete set of elastic moduli in single-crystal minerals at extremely high *P*-*T* conditions (e.g. Fan et al. 2015a; Mao et al. 2015; Murakami et al. 2007; Yang et al. 2015; Zhang et al. 2016). There have been a number of single-crystal elasticity studies on pyrope at ambient conditions (e.g. Leitner et al. 1980; O'Neill et al. 1991), high pressure (e.g. Conrad et al. 1999; Sinogeikin and Bass 2000), and high temperature (e.g. Sinogeikin and Bass 2002) conditions using BLS technique. Recently, Lu et al.

This is a preprint, the final version is subject to change, of the American Mineralogist (MSA)
Cite as Authors (Year) Title. American Mineralogist, in press.
DOI: https://doi.org/10.2138/am-2019-6897

(2013) measured the single-crystal elasticity of Fe-bearing pyrope at high *P-T* conditions using BLS technique, which provided the detailed description of Fe effect on the elastic moduli of pyrope.

Furthermore, the effect of hydrogen on the elasticity of other major mantle minerals (e.g. olivine, wadsleyite, and ringwoodite) has been studied extensively at ambient and high pressure/high temperature conditions (e.g. Inoue et al. 1998; Jacobsen et al. 2004, 2008; Mao et al. 2008, 2010, 2011, 2012; Sinogeikin et al. 2003; Wang et al. 2003, 2006). However, there is only one study on the acoustic velocities and single-crystal elastic moduli of hydrous pyrope (~180 ppmw) using BLS technique at ambient conditions (O'Neill et al. 1991). The effect of hydration on the acoustic velocities and elastic moduli of pyrope at high *P-T* conditions remains unavailable, even though it is highly desirable to use its single-crystal elasticity for understanding the geodynamic processes of the upper mantle. Up to now, only Fan et al. (2017b) conducted the high *P-T* equation of state study of hydrous pyrope using synchrotron-based XRD technique.

In this study, we measured the acoustic velocities (V_P and V_S) of single-crystal hydrous pyrope at high pressures up to ~18.6 GPa and high temperatures up to 700 K using BLS technique, and derived its full set of single-crystal elastic moduli at high *P-T* conditions. Based on our results, we further evaluated the effects of hydrogen on the elastic moduli, sound velocities, and elastic anisotropies of pyrope. Finally, we applied our results to discuss the hydrogen effect on the velocity profile and V_P/V_S ratio of pyrope in the Earth's upper mantle.

EXPERIMENTAL METHODS

The single-crystal hydrous pyrope was synthesized in a multi-anvil pressure apparatus (YJ-3000T), at the Institute of Geochemistry, Chinese Academy of Sciences, Guiyang, China. More detailed information about the sample synthesis and sample characterization were presented elsewhere by Fan et al. (2017b). Here we briefly report results from Electron probe microanalysis (EPMA), Fourier transform infrared

(FTIR), and XRD. EPMA results show that our sample is homogeneous with a chemical formula as $Mg_{3.006}Al_{1.995}Si_{3.005}O_{12}$. Hydrogen concentrations were determined by FTIR spectroscopy and the absorption bands were readily attributed to structural bonded hydroxyl groups in pyrope (Geiger et al. 1991; Mookherjee and Karato 2010; Withers et al. 1998). The water content in our sample was determined to be ~900(±100) ppmw using the formula of Bell et al. (1995). Meanwhile, the XRD pattern of our sample confirmed a cubic structure with lattice parameter a=11.460(3) Å at ambient conditions, yielded the unit-cell volume V_0=1505.24(8) Å^3 and density ρ=3.557(4) g/cm^3. The unit-cell volume of our hydrous pyrope at ambient conditions is ~0.15% higher than anhydrous pyrope (Du et al. 2015; Zhang et al. 1998), which agrees with previous studies for other mantle minerals (e.g. Holl et al. 2008; Smyth et al. 2003; Smyth and Jacobsen 2006; Ye et al. 2010, 2012).

Pyrope has a cubic structure with only three independent elastic moduli (C_{11}, C_{12}, and C_{44}), and therefore, a single crystallographic orientation is sufficient to constrain all three of them using BLS measurements. The crystallographic plane of sample piece is (0.34, -0.53, 0.92) determined by single-crystal XRD at beamline 13-BMD of the GeoSoilEnviroConsortium for Advanced Radiation Sources (GSECARS) of Advanced Photon Source (APS), Argonne National Laboratory (ANL). We double-sides polished our sample pieces to ~20-30 μm thickness with successively finer grits down to a final 3M diamond lapping film of 1 μm grainsize. The thinly polished platelet was then cleaved into several square pieces of the desired size (~150 μm) for high-pressure/high temperature measurements.

High-pressure BLS combined with XRD measurements were conducted on the single-crystal hydrous pyrope in a short symmetrical DAC at 13-BMD beamline of APS. An incident X-ray beam of 0.3344 Å wavelength focused to a 3×7 μm^2 area was used to determine the unit-cell volume of crystal in the DACs. Round Re gasket of 250 μm thick and 3 mm in diameter was pre-indented to ~55 μm thickness using a pair of 500 μm culet size diamond anvils. Subsequently, a cylindrical 300 μm

diameter hole was drilled in the pre-indented area as the sample chamber. A single-crystal platelet with a diameter of ~150 μm was then placed into the sample chamber, together with some ruby spheres of approximately 5 μm in diameter as the pressure indicator (Mao et al. 1986) for neon gas loading as well as for high-pressure experiments. The neon pressure medium was loaded into the sample chamber using the gas-loading system at GSECARS of APS (Rivers et al. 2008). Pressures were measured from ruby fluorescence spectra, while pressure uncertainties were calculated using multiple measurements before and after collection of BLS spectra for each pressure point. The XRD spectra were used to determine density at each pressure before and after BLS measurements (Table 1).

High-temperature BLS experiments were also performed at 13-BMD beamline of APS. A single-crystal hydrous pyrope (~150 μm) was loaded into an externally-heated DAC (EHDAC), which was equipped with an alumina ceramic heater coiled with two Pt wires of 200 μm in diameter and 48 cm in length (Fan et al. 2019; Kantor et al. 2012; Lu et al. 2013; Mao et al. 2015; Yang et al. 2014, 2016). Re was used as the gasket material and pre-indented to ~55 μm thickness using a pair of diamond anvils with 500 μm culet size and then a 300 μm diameter sample chamber was drilled at the center of pre-indentation. The single-crystal hydrous pyrope sample was sealed in the sample chamber. An R-type thermocouple was attached to one of diamond surface approximately 500 μm away from its culet and clad with a ceramic adhesive (Resbond 920) for temperature measurements. To minimize temperature instability for each heating run, we firstly heated the sample chamber to a given temperature and then kept it at this temperature for at least 30 minutes. Temperatures of the sample chamber were actively stabilized within ±1 K using the temperature-power feedback program with a remotely controlled Tektronix Keithley DC power supply during the experiments (Sinogeikin et al. 2006). Single-crystal XRD patterns of hydrous pyrope before and after BLS measurements were also collected to determine the lattice parameters and densities of the sample at high

195 temperatures (Table 2). Temperatures were increased every 100 K from room
196 temperature (300 K) to maximum temperature (700 K), and then decreased to room
197 temperature to check for possible changes in the lattice parameters and elastic moduli
198 at ambient conditions. From Table 2, we can find that the lattice parameters and
199 elastic moduli at ambient conditions of our hydrous pyrope are highly consistent
200 before and after heating. In addition, we did not measure the water content of our
201 sample after the high-temperature BLS measurements due to the relatively small size
202 and thickness of our sample. However, the previous study has determined the water
203 content of the hydrous garnet after heating up to ~ 1273 K and indicated the water
204 loss of hydrous sample less than 10% (Dai et al. 2012). The maximum experimental
205 temperature in this study (~ 700 K) is significantly lower than that in previous study
206 (~ 1273 K) (Dai et al. 2012). Therefore, we infer that there is no obvious water loss
207 during the high temperature BLS measurements in this study, which is also consistent
208 with the previous study that demonstrated that the intrinsic hydrogen loss in hydrous
209 pyrope occurs at temperatures of ≥ 500 °C (Bell et al. 1995).

210 The Brillouin system at 13-BMD beamline was equipped with a Coherent Verdi V2
211 solid-state laser with a wavelength of 532 nm, a Perkin-Elmer photomultiplier
212 detector (model: MP983), and a JRS six-pass tandem Fabry-Pérot interferometer (Lu
213 et al. 2013; Yang et al. 2014). BLS spectra were collected in the symmetric forward
214 scattering geometry with an external scattering angle of 50°, which was calibrated
215 using the elastic moduli of standard silicate glass, distilled water, and single-crystal
216 MgO (Ostwald et al. 1977; Polian et al. 2002; Sinogeikin and Bass 2000). The laser
217 beam focused on the sample position was approximately 15 μm in diameter. The
218 acoustic velocities (V_P and V_S) of our sample were derived from analysis of the
219 measured Brillouin frequency shift as follows:

220 $$V_{P,S} = \frac{\lambda_0 \Delta \nu_B}{2 \sin\frac{\theta}{2}} \quad (1)$$

This is a preprint, the final version is subject to change, of the American Mineralogist (MSA)
Cite as Authors (Year) Title. American Mineralogist, in press.
DOI: https://doi.org/10.2138/am-2019-6897

where $V_{P,S}$ is the acoustic velocities, λ_0 is the incident laser wavelength, $\Delta\nu_B$ is the Brillouin frequency shift, and θ is the external scattering angle.

RESULTS AND DATA ANALYSES

BLS and XRD spectra of single-crystal hydrous pyrope sample are collected up to ~18.6 GPa at room temperature in 2-3 GPa pressure interval and up to 700 K at room pressure in 100 K temperature interval. For all of the Brillouin spectra, one quasi-longitudinal and one quasi-transverse acoustic mode are observed. Typical Brillouin spectra at high pressure/high temperature conditions are shown in Figure 1. The measured frequency shifts are converted to velocities along the horizontal axis using equation (1). Most spectra show strong V_P and V_S peaks with high signal-to-noise ratios except for some crystallographic directions where V_P peaks are weakly observable (Fig. 1). Brillouin signals of neon pressure medium are also observed at pressures below ~8 GPa, but they are too weak to be seen when the pressures are increased above 8 GPa. For each platelet at each given *P*-*T* conditions, Brillouin spectra are collected in 19 different crystallographic directions from 0 to 180° of the azimuthal angle at every 10° (Fig. 2). The variation in measured V_P and V_S as a function of azimuthal angle are not observed outside experimental uncertainties, indicating that our hydrous pyrope is almost elastically isotropic at ambient and high pressure/high temperature conditions (Fig. 2). Furthermore, both V_P and V_S of hydrous pyrope increase with increasing pressure, and decrease with increasing temperature.

Individual elastic moduli (C_{ij}) of single-crystal hydrous pyrope at each given pressure/temperature conditions (Tables 1 and 2) are obtained by fitting the measured spatial dispersion (velocity vs. orientation) of V_P and V_S to Christoffel's equation using non-linear least square method (Every 1980):

$$\left|C_{ijkl}n_j n_l - \rho {V_{P,S}}^2 \delta_{ik}\right| = 0 \quad (2)$$

where C_{ijkl} are the elastic constant in full suffix notation, n_j and n_l are the direction cosines of the phonon along the propagation direction, ρ is the density at each pressure/temperature condition, δ_{ik} is the Kronecker delta function. The

This is a preprint, the final version is subject to change, of the American Mineralogist (MSA)
Cite as Authors (Year) Title. American Mineralogist, in press.
DOI: https://doi.org/10.2138/am-2019-6897

root-mean-square (RMS) deviation of the fitting are about 20 m/s, indicating excellent agreement between measured and calculated sound velocities at ambient and high pressure/temperature conditions (Fig. 2). Previous studies also indicated that the single-crystal elastic moduli of pyrope could be calculated by averaging the measured acoustic velocities (e.g. Lu et al. 2013; Sinogeikin and Bass 2000). From Table S1, we notice that the single-crystal elastic moduli of hydrous pyrope derived from the non-linear least-squares fitting are indistinguishable within their uncertainties from those calculated values by averaging the measured acoustic velocities assuming that pyrope is elastically isotropic. All of the individual elastic moduli (C_{11}, C_{12}, and C_{44}) for hydrous pyrope increase smoothly with increasing pressure, and decrease with increasing temperature (Fig. 3).

Using the derived individual elastic moduli (C_{11}, C_{12}, and C_{44}) of hydrous pyrope, the adiabatic bulk and shear moduli (K_S and G) are calculated according to the Voigt-Reuss-Hill averages (Hill 1952). The aggregate adiabatic bulk (K_{S0}) and shear moduli (G_0) of hydrous pyrope at ambient conditions are 168.6(4) and 92.0(3) GPa, respectively. The pressure derivatives of elastic moduli at 300 K (Tables 3 and 4) are obtained by fitting the elastic moduli at high pressure using the third-order Eulerian finite-strain equation (Figs. 3a and 4a) (Birch 1978). The pressure derivatives of the individual (C_{ij}) and aggregate (K_S and G) elastic moduli at room temperature are derived to be $(\partial C_{11}/\partial P)_T$=6.2(1), $(\partial C_{12}/\partial P)_T$=3.7(1), $(\partial C_{44}/\partial P)_T$=1.5(1), $(\partial K_S/\partial P)_T$=4.6(1), and $(\partial G/\partial P)_T$=1.3(1), respectively. Due to the limited temperature range for high-temperature data, a linear equation is applied to obtain the temperature derivatives of elastic moduli (Figs. 3b and 4b). The temperature derivative of individual and aggregate elastic moduli at ambient pressure (Tables 3 and 4) are derived to be $(\partial C_{11}/\partial T)_P$=-0.028(1) GPa/K, $(\partial C_{12}/\partial T)_P$=-0.009(1) GPa/K, $(\partial C_{44}/\partial T)_P$=-0.006(1) GPa/K, $(\partial K_S/\partial T)_P$=-0.015(1) GPa/K, and $(\partial G/\partial T)_P$=-0.008(1) GPa/K, respectively. The aggregate V_P and V_S of our hydrous pyrope at high pressure/temperature conditions (Fig. 5) are calculated using the following equations:

This is a preprint, the final version is subject to change, of the American Mineralogist (MSA)
Cite as Authors (Year) Title. American Mineralogist, in press.
DOI: https://doi.org/10.2138/am-2019-6897

$$V_{\mathrm{P}} = \sqrt{\frac{K_{\mathrm{S}} + \frac{4G}{3}}{\rho}} \quad (3)$$

$$V_{\mathrm{S}} = \sqrt{\frac{G}{\rho}} \quad (4)$$

DISCUSSION

Hydrogen effect on the elasticity of pyrope at high *P-T* conditions

In order to understand the effect of hydrogen on the elasticity of pyrope, we compare our results with literature values for pyrope obtained from BLS and ultrasonic interferometer measurements. Tables 3 and 4 show a complete list of individual (C_{ij}s) and aggregate (K_{S0} and G_0) elastic moduli obtained in the present study for hydrous pyrope along with those previous studies of anhydrous pyrope. Compared to anhydrous pyrope (e.g. Sinogeikin and Bass 2000, 2002a) (Table 3), the addition of ~900 ppmw H_2O in our pyrope sample has negligible effects on the individual elastic moduli C_{ij} values at ambient conditions within experimental uncertainties. Our aggregate bulk, K_{S0}, and shear moduli, G_0, at ambient conditions of hydrous pyrope are 168.6(4) and 92.0(3) GPa, respectively (Table 4). The presence of ~900 ppmw H_2O in our hydrous pyrope also does not affect the values of K_{S0} and G_0 within experimental uncertainties compared to anhydrous pyrope (Table 4). This is consistent with the conclusion from the study by O'Neill et al. (1991), who deduced that there might have no discernable effect of hydrogen on the elastic properties of pyrope at ambient conditions, though the water solubility in their hydrous pyrope is significantly smaller (~180 ppmw H_2O) than our hydrous pyrope (~900 ppmw H_2O).

Our results also show that hydration has no visible effect on the pressure and temperature derivatives of C_{ij}s in pyrope within experimental uncertainties (Table 3). This is clearly different from the effect of composition (e.g. Fe and Ca) on the temperature derivatives of C_{ij}s in pyrope-rich garnet, where a distinctly larger temperature derivative of C_{12} and lower temperature derivative of C_{11} and C_{44} for (Fe,Ca)-bearing pyrope-rich garnet reported by Lu et al. (2013).

The $(\partial K_S/\partial P)_T$ of our hydrous pyrope is 4.6 (Fig. 4 and Table 4), which is slightly higher than most results of anhydrous pyropes [$(\partial K_S/\partial P)_T$=4.1-4.51] (Table 4), except a distinctly lower value ($(\partial K_S/\partial P)_T$=3.2) reported by Conrad et al. (2000) and higher value ($(\partial K_S/\partial P)_T$=5.3) reported by Chen et al. (1999). Moreover, the $(\partial G/\partial P)_T$ of our hydrous pyrope ($(\partial G/\partial P)_T$=1.3) is indistinguishable from most previous studies ($(\partial G/\partial P)_T$=1.3-1.5) on anhydrous pyrope within experimental uncertainties, except for two slightly higher values ($(\partial G/\partial P)_T$=1.66 and 1.7) reported from ultrasonic interferometry experiments by Gwanmesia et al. (2006) and Chantel et al. (2016), respectively. Furthermore, our derived $(\partial K_S/\partial T)_P$ and $(\partial G/\partial T)_P$ of hydrous pyrope are indistinguishable from previous BLS values for anhydrous pyrope within their uncertainties, but their absolute values appeared to be slightly lower than most of those from ultrasonic interferometry measurements except a consistent $(\partial G/\partial T)_P$ absolute value reported by Chantel et al. (2016) (Table 4). Therefore, we conclude that the presence of ~900 ppmw H_2O in our pyrope slightly enhances the $(\partial K_S/\partial P)_T$, but does not distinctly affect the K_{S0}, G_0, $(\partial G/\partial P)_T$, $(\partial K_S/\partial T)_P$, and $(\partial G/\partial T)_P$ within their uncertainties.

Hydrogen effect on the elastic anisotropy of pyrope at high *P-T* conditions

Elastic wave anisotropy is a critical feature of the upper mantle (e.g. Karato 1998). One advantage of using single-crystal samples in BLS is that we can obtain the full elastic moduli and put a constraint on the elastic anisotropy. The elastic anisotropy of minerals expresses the difference in stiffness of materials in different crystallographic directions, which can provide insights into seismic anisotropy and can be an indicator of the mechanical stability of materials (e.g. Hu et al. 2016; Sinogeikin and Bass 2000). Thus, knowledge of elastic anisotropy for hydrous pyrope at high *P-T* may shed light on understanding the seismic anisotropy within the Earth's upper mantle.

For the cubic pyrope, the elastic anisotropy factor (A) can be expressed as (Karki et al. 1997; Sinogeikin and Bass 2000):

330 $$A = \frac{2C_{44}+C_{12}}{C_{11}} - 1 \quad (5)$$

331 where A indicates the deviation from elastic isotropy, with A=0 for an elastically
332 isotropic material. Analysis of these parameters using our data show that the absolute
333 A values of our hydrous pyrope slightly decreases with increasing pressure and
334 temperature, where A are -0.026 at ambient pressure, 0.001 at 18.53 GPa, and -0.019
335 at 700 K. Moreover, our hydrous pyrope at ambient conditions has slightly higher
336 absolute A value than anhydrous pyrope (A=-0.006 to -0.008) (e.g. Sinogeikin and
337 Bass, 2000, 2002a; O'Neill et al. 1991). However, all these absolute A values are still
338 pretty small and very close to zero. Thus, our results indicate that hydrogen does not
339 have a significant effect on the elastic anisotropy of pyrope. Hydrous pyrope remains
340 elastically isotropic at high pressure/high temperature conditions compared to the
341 other (olivine, orthopyroxene, and clinopyroxene) major minerals in the upper mantle
342 (e.g. Mao et al. 2015; Sang et al. 2014; Zhang et al. 2016). Therefore, pyrope may not
343 have a significant contribution to seismic anisotropy in the upper mantle, at least
344 when its water content is less than 900 ppmw.

345 **IMPLICATION**

346 **Hydrogen effect on the velocity profiles of pyrope in the Earth's upper mantle**

347 The NAMs in the Earth's deep mantle may serve as a large internal reservoir of
348 water and are important for understanding the evolution and dynamics of Earth's
349 interior (e.g. Bell and Rossman 1992a; Beran and Libowitzky 2006; Ohtani 2005,
350 2015). Hydration of NAMs has been proposed to correlate with the observed velocity
351 anomalies in the Earth's mantle (e.g. Nolet and Zielhuis 1994; Ohtani 2005; Song et
352 al. 2004; van der Meijde et al. 2003). With the obtained elastic moduli of hydrous
353 pyrope at high P-T conditions in this study, we evaluate the effect of hydration on the
354 sound velocities of pyrope at upper mantle conditions.

355 The presence of ~900 ppmw water in pyrope lowers its V_P and V_S by ~0.7% at
356 ambient conditions (Sinogeikin and Bass 2000). Furthermore, for a better

This is a preprint, the final version is subject to change, of the American Mineralogist (MSA)
Cite as Authors (Year) Title. American Mineralogist, in press.
DOI: https://doi.org/10.2138/am-2019-6897

357 understanding of the hydrogen influence on the velocity behavior of pyrope, we have
358 modeled the velocity profiles of hydrous pyrope along the upper mantle geotherm
359 (Katsura et al. 2010) and a cold subducted slabs geotherm (Eberle et al. 2002) using
360 the updated high-P/T elasticity results. Our modeling here is limited to the
361 upper-mantle region ranging from 200 km to 400 km depth because of the much more
362 complex mineralogical, geochemical, and seismic heterogeneities above 200 km
363 depth (e.g. Jordan 1975; Grand and Helmberger 1984). The modeled results are then
364 compared with the velocity profiles of anhydrous pyrope (Sinogeikin and Bass 2000,
365 2002a) and (Fe, Ca)-bearing pyrope-rich garnet (Lu et al. 2013). Briefly, the
366 third-order Eulerian finite-strain equation and the third-order Birch-Murnaghan
367 equation of state (Birch 1978) are used to obtain the K_S, G, V_P and V_S of relevant
368 minerals by extrapolating the experimentally-derived elastic moduli and their P-T
369 derivatives to relevant P-T conditions (see Lu et al. 2013 for details). By allowing
370 elastic parameters to vary within their plausible ranges, the uncertainties ($\pm 1\sigma$) of
371 extrapolation results can also be estimated.

372 Figure 6 shows the calculated velocity-depth relationships of hydrous pyrope along
373 with those of anhydrous phase. Because of larger pressure derivative of K_S and similar
374 temperature derivative of K_S, the V_P of hydrous pyrope increases more rapidly with
375 depth than that of anhydrous pyrope. Moreover, the V_P of hydrous pyrope crosses and
376 exceeds that of anhydrous phase at ~200 km and ~270 km depth along the upper
377 mantle geotherm and the cold subducted slabs geotherm, respectively. However,
378 considering the error bars presented in Fig. 6, the V_P profiles are indistinguishable
379 between hydrous and anhydrous pyrope at 200-400 km depth. Similarly, due to the
380 small effects of hydrogen on the pressure derivative of G, the difference in the V_S
381 between hydrous and anhydrous pyrope is also within the uncertainties over the
382 200-400 km depth.

383 On the other hand, hydrogen can enhance the anelasticity (e.g. Karato 1995) and
384 may further change the V_P and V_S. Combining the anelastic effect, the change of V_P

This is a preprint, the final version is subject to change, of the American Mineralogist (MSA)
Cite as Authors (Year) Title. American Mineralogist, in press.
DOI: https://doi.org/10.2138/am-2019-6897

and V_S associated with ~900 ppmw H_2O in pyrope at the Earth's upper mantle may be greater than that observed here. However, although up to several hundred ppmw H_2O have been found in some natural garnets (e.g. Aines and Rossman 1984a, 1984b; Li H Y et al. 2018), most of the mantle-derived garnets typically contain <100 ppmw H_2O (e.g. Beran and Libowitzky 2006; Ohtani 2015). Combined with the limited effect of ~900 ppmw H_2O on the velocities of pyrope, we thus infer that hydrogen has no significant effect on the velocity profiles of pyrope at upper mantle conditions. Nevertheless, compared to the effect of hydrogen on the velocities of pyrope, the effect of compositions (e.g. Fe and Ca) is significant. Accordingly, the velocity reduction produced by the effect of Fe and Ca is ~2-3% either along the upper mantle geotherm or along the cold subducted slabs geotherm (Fig. 6). Therefore, the elasticity studies of hydrous (Fe, Ca)-bearing pyrope-rich garnet at high *P-T* conditions are needed to provide a more comprehensive understanding of the coupled effect of compositions (e.g. Fe and Ca) and hydration on the elasticity and velocity profiles of garnet and then the Earth's upper mantle.

Hydrogen effect on the V_P/V_S ratio of pyrope in the Earth's upper mantle

The V_P/V_S ratio has been proposed as one of the possible indicators to determine the composition in the deep Earth (e.g. Anderson and Bass 1984; Duan et al. 2018; Li and Neuville 2010; Mao et al. 2010), such as the silica content of continental crust (Christensen 1996). It has been widely used to infer the thermal and compositional state of the upper mantle (e.g. Afonso et al. 2010; Chou et al. 2009; Lee 2003; Niu et al. 2004; Speziale et al. 2005). Here, we have investigated the effect of hydration on the V_P/V_S ratio of pyrope. The V_P/V_S ratio of the hydrous pyrope at ambient conditions is 1.78, which is the same with the anhydrous pyrope (1.78) (Sinogeikin and Bass 2000). The V_P/V_S ratio increases with pressure at an average rate of 5.03×10^{-3} GPa^{-1}, but it remains constant with increasing temperature from 300 K to 700 K. At the depth of 400 km, the V_P/V_S ratio of the hydrous pyrope increases to 1.86 along the upper mantle geotherm and to 1.85 along the cold subducted slabs geotherm, which are ~0.5%

higher than that of the anhydrous phase. A similar increase in the V_P/V_S ratio caused by hydration was observed for ringwoodite (Jacobsen and Smyth 2006; Sinogeikin et al. 2003). However, this contrasts with the behavior of olivine for which a ~0.7% decreased in the V_P/V_S ratio was observed in the hydrous olivine relative to anhydrous phase (Mao et al. 2010; Zha et al. 1996). Figure 7 also shows a comparison of the V_P/V_S ratio for hydrous and anhydrous pyrope with the (Fe,Ca)-bearing pyrope-rich garnet. We notice although all garnets exhibit the increased V_P/V_S ratio with increasing depths, the hydrous pyrope has the highest value throughout the upper mantle depths. However, considering the uncertainties of the V_P/V_S ratio presented in Fig. 7, the variation of the V_P/V_S ratio among these garnet samples should be limited at 200-400 km depth. This confirms the results of the previous study, which indicated that the variation of mineral composition has only a weak effect on the V_P/V_S ratio of the upper mantle (Duan et al. 2018). Finally, we infer that the hydrogen has also no significant effect on the V_P/V_S ratio of pyrope at upper mantle conditions, especially for the limited hydration level (<100 ppmw H_2O) of mantle-derived garnets.

Acknowledgments

We would like to thank two anonymous reviewers for their thorough and helpful comments and Prof. Jennifer Kung for handling this paper. We also thank Z. Mao for providing the Igor fitting code. D. W. Fan acknowledges financial support from the National Natural Science Foundation of China (41772043), the Joint Research Fund in Huge Scientific Equipment (U1632112) under the cooperative agreement between NSFC and CAS, CAS "Light of West China" Program (Dawei Fan, 2017), and Youth Innovation Promotion Association CAS (Dawei Fan, 2018434). J. G. Xu acknowledges financial support from the National Natural Science Foundation of China (41802043), and China Postdoctoral Science Foundation (Grant No. 2018M631104). This work was performed at GeoSoilEnviroCARS (The University of Chicago, Sector 13), Advanced Photon Source (APS), Argonne National Laboratory. GeoSoilEnviroCARS is supported by the National Science Foundation (EAR-0622171) and the Department of Energy (DE-FG02-94ER14466) under Contract No. DE-AC02-06CH11357. This research used resources at the Advanced Photon

441 Source, a U.S. Department of Energy (DOE) Office of Science User Facility operated for the DOE
442 Office of Science by Argonne National Laboratory under Contract No. DE-AC02-06CH11357.

443 REFERENCES CITED

444 Ackermann, L., Cemič, L, and Langer, K. (1983) Hydrogarnet substitution in pyrope: a possible
445 location for "water" in the mantle. Earth and Planetary Science Letters, 62, 208-214.

446 Afonso, J.C., Ranalli, G., Fernàndez, M., Griffin, W.L., O'Reilly, S.Y., and Faul, U. (2010) On
447 the V_P/V_S–Mg# correlation in mantle peridotites: Implications for the identification of thermal
448 and compositional anomalies in the upper mantle. Earth and Planetary Science Letters, 289,
449 606-618.

450 Aines, R., and Rossman, G.R. (1984a) The hydrous component in garnets: pyralspites. American
451 Mineralogist, 69, 1116-1126.

452 Aines, R., and Rossman, G.R. (1984b) Water content of mantle garnets. Geology, 12, 720-723.

453 Anderson, D.L. (1989) Composition of the Earth. Science, 243, 367-370.

454 Anderson, D.L., and Bass, J.D. (1984) Mineralogy and composition of the upper mantle.
455 Geophysical Research Letters, 11, 637-640.

456 Bass, J.D., and Anderson, D.L. (1984) Composition of the upper mantle: geophysical tests of two
457 petrological models. Geophysical Research Letters, 11, 229-232.

458 Bass, J.D., and Zhang, J.S. (2015) Theory and practice: techniques for measuring high-P–T
459 elasticity. Treatise on Geophysics (Second Edition), 2, 293-312.

460 Bass, J.D., Sinogeikin, S.V., and Li, B. (2008) Elastic properties of minerals: A key for
461 understanding the composition and temperature of Earth's interior. Elements, 4, 165-170.

462 Bell, D.R., Ihinger, P.D., and Rossman, G.R. (1995) Quantitative analysis of trace OH in garnet
463 and pyroxenes. American Mineralogist, 80, 465-474.

464 Bell, D.R., and Rossman, G.R. (1992a) Water in Earth's mantle: The role of nominally anhydrous
465 minerals. Science, 255, 1391-1397.

466 Bell, D.R., and Rossman, G.R. (1992b) The distribution of hydroxyl in garnets form the
467 subcontinental mantle of southern Africa. Contributions to Mineralogy and Petrology, 111,
468 161-178.

469 Beran, A., and Libowitzky, E. (2006) Water in natural mantle minerals II: olivine, garnet and
470 accessory minerals. Reviews in Mineralogy and Geochemistry, 62, 169-191.

471 Bina, C.R. (2013) Mineralogy: Garnet goes hungry. Nature Geoscience, 6, 335-336.

472 Birch, F. (1978) Finite strain isotherm and velocities for single-crystal and polycrystalline NaCl at
473 high pressure and 300 K. Journal of Geophysical Research, 83, 1257-1268.

474 Bolfan-Casanova, N., Keppler, H., and Rubie, D.C. (2000) Water partitioning between nominally
475 anhydrous minerals in the MgO-SiO_2-H_2O system up to 24 GPa: implications for the
476 distribution of water in the Earth's mantle. Earth and Planetary Science Letters, 182, 209-221.

477 Chantel, J., Manthilake, G.M., Frost, D.J., Beyer, C., Ballaran, T.B., Jing, Z.C., Wang, Y.B. (2016)
478 Elastic wave velocities in polycrystalline $Mg_3Al_2Si_3O_{12}$-pyrope garnet to 24 GPa and 1300 K.
479 American Mineralogist, 101, 991-997.

480 Chen, G.L., Miletich, R., Mueller, K., and Spetzler, H.A. (1997) Shear and compressional mode
481 measurements with GHz ultrasonic interferometry and velocity-composition systematics for the
482 pyrope-almandine solid solution series. Physics of the Earth and Planetary Interiors, 99,
483 273-287.

484 Chen, G.L., Cooke, J.A.Jr., Gwanmesia, G.D., Liebermann, R.C. (1999) Elastic wave velocities of
485 $Mg_3Al_2Si_3O_{12}$-pyrope garnet to 10 GPa. American Mineralogist, 84, 384-388.

486 Christensen, N.I. (1996) Poisson's ratio and crustal seismology. Journal of Geophysical Research,
487 101, 3139-3156.

488 Conrad, P.G., Zha, C.S., Mao, H.K., and Hemley, R.J. (1999) The high-pressure, single-crystal
489 elasticity of pyrope, grossular, and andradite. American Mineralogist, 84, 374-383.

490 Dai, L.D., Li, H.P., Hu, H.Y., Shan, S.M., Jiang, J.J., and Hui, K.S. (2012) The effect of chemical
491 composition and oxygen fugacity on the electrical conductivity of dry and hydrous garnet at
492 high temperatures and pressures. Contributions to Mineralogy and Petrology, 163, 689-700.

493 Du, W., Clark, S.M., Walker, D. (2015) Thermo-compression of pyrope-grossular garnet solid
494 solutions: non-linear compositional dependence. American Mineralogist, 100, 215-222.

495 Duan, Y.F., Li, X.Y., Sun, N.Y., Ni, H.W., Tkachev. S.N., and Mao, Z. (2018) Single-crystal
496 elasticity of $MgAl_2O_4$-spinel up to 10.9 GPa and 1000 K: Implication for the velocity structure
497 of the top upper mantle. Earth and Planetary Science Letters, 481, 41-47.

498 Duffy, T.S., and Anderson, D.L. (1989) Seismic velocities in mantle minerals and the mineralogy
499 of the upper mantle. Journal of Geophysical Research, 94, 1895-1912.

500 Eberle, M.A., Grasset, O., and Sotin, C. (2002) A numerical study of the interaction between the
501 mantle wedge, subducting slab, and overriding plate. Physics of the Earth and Planetary
502 Interiors, 134, 191-202.

503 Every, A. (1980) General closed-form expressions for acoustic waves in elastically anisotropic
504 solids. Physical Review B, 22, 1746-1760.

505 Fan, D.W., Fu, S.Y., Yang, J., Tkachev, S.N., Prakapenka, V.B., and Lin, J.F. (2019) Elasticity of
506 single-crystal periclase at high pressure and temperature: the effect of iron on the elasticity and
507 seismic parameters of ferropericlase in the lower mantle. American Mineralogist, 104, 262-275.

508 Fan, D.W., Kuang, Y.Q., Xu, J.G., Li, B., Zhou, W.G., and Xie, H.S. (2017a) Thermoelastic
509 properties of grossular–andradite solid solution at high pressures and temperatures. Physics and
510 Chemistry of Minerals, 44, 137-147.

511 Fan, D.W., Lu, C., Xu, J.G., Yan, B.M., Yang, B., and Chen, J.H. (2017b) Effects of water on
512 P-V-T equation of state of pyrope. Physics of the Earth and Planetary Interiors, 267, 9-18.

513 Fan, D.W., Ma, M.N., Wei, S.Y., Chen, Z.Q., and Xie, H.S. (2013) High pressure elastic behavior
514 of synthetic $Mg_3Y_2(SiO_4)_3$ garnet up to 9GPa. Advances in Materials Science and Engineering,
515 2013, 502702.

Fan, D.W., Mao, Z., Yang, and J., Lin, J.F. (2015a) Determination of the full elastic tensor of single crystals using shear wave velocities by Brillouin spectroscopy. American Mineralogist, 100, 2590-2601.

Fan, D.W., Wei, S.Y., Liu, J., Li, Y.C., and Xie, H.S. (2011) High pressure X-ray diffraction study of a grossular-andradite solid solution and the bulk modulus variation along this solid solution. Chinese Physics Letters, 28, 076101.

Fan, D.W., Xu, J.G., Ma, M.N., Liu, J., and Xie, H.S. (2015b) *P–V–T* equation of state of spessartine-almandine solid solution measured using a diamond anvil cell and in situ synchrotron X‐ray diffraction. Physics and Chemistry of Minerals, 42, 63-72.

Fan, D.W., Xu, J.G., Ma, M.N., Wei, S.Y., Zhang, B., Liu, J., and Xie, H.S. (2015c) *P-V-T* equation of state of $Ca_3Cr_2Si_3O_{12}$ uvarovite garnet by using a diamond-anvil cell and in-situ synchrotron X-ray diffraction. American Mineralogist, 100, 588-597.

Fan, D.W., Zhou, W.G., Liu, C.Q., Liu, Y.G., Wan, F., Xing, Y.S., Liu, J., Bai, L.G., and Xie, H.S. (2009) The thermal equation of state of $(Fe_{0.86}Mg_{0.07}Mn_{0.07})_3Al_2Si_3O_{12}$ almandine. Mineralogical Magazine, 73, 95-102.

Frost, D.J. (2008) The upper mantle and transition zone. Elements, 4, 171-176.

Geiger, C.A., Langer, K., Bell, D.R., Rossman, G.R., and Winkler, B. (1991) The hydroxide component in synthetic pyrope. American Mineralogist, 76, 49-59.

Grand, S.P., and Helmberger, D.V. (1984) Upper mantle shear structure of North America. Geophysical Journal International, 76, 399-438.

Gwanmesia, G.D., Jackson, I., and Liebermann, R.C. (2007) In search of the mixed derivative $\partial^2 M/\partial P\partial T$ (M=G, K): joint analysis of ultrasonic data for polycrystalline pyrope from gas- and solid-medium apparatus. Physics and Chemistry of Minerals, 34, 85-93.

Gwanmesia, G.D., Zhang, J.Z., Darling, K., Kung, J., Li, B.S., Wang, L.P., Neuville, D., Liebermann, R.C. (2006) Elasticity of polycrystalline pyrope ($Mg_3Al_2Si_3O_{12}$) to 9 GPa and 1000 °C. Physics of the Earth and Planetary Interiors, 155, 179-190.

542 Herzberg C., and Gasparik T. (1991) Garnet and pyroxenes in the mantle: A test of the majorite
543 fractionation hypothesis. Journal of Geophysical Research, 96, 16263-16274.

544 Hill, R. (1952) The elastic behaviour of a crystalline aggregate. Proceedings of the Physical
545 Society-Section A, 65, 349-354.

546 Hirschmann, M. (2006) Water, melting, and the deep earth H_2O cycle. Annual Review of Earth
547 and Planetary Sciences, 34, 629-653.

548 Hirschamann, M., and Kohlstedt, D. (2012) Water in Earth's mantle. Physics Today, 65, 40-45.

549 Holl, C.M., Smyth, J.R., Jacobsen, S.D., Frost, D.J. (2008) Effects of hydration on the structure
550 and compressibility of wadsleyite, β-(Mg_2SiO_4). American Mineralogist, 93, 598-607.

551 Hu, Y., Wu, Z.Q., Dera, P.K., and Bina, C.R. (2016) Thermodynamic and elastic properties of
552 pyrope at high pressure and high temperature by first-principles calculations. Journal of
553 Geophysical Research, 121, 6462-6476.

554 Ingrin, J. and Skogby, H. (2000) Hydrogen in nominally anhydrous upper-mantle minerals:
555 concentration levels and implications. European Journal of Mineralogy, 12, 543-570.

556 Inoue, T., Weidner, D.J., Northrup, P.A., and Parise, J.B. (1998) Elastic properties of hydrous
557 ringwoodite (γ-phase) in Mg2SiO4. Earth and Planetary Science Letters, 160, 107-113.

558 Ita, J., and Stixrude, L. (1992) Petrology, elasticity, and composition of the mantle transition zone.
559 Journal of Geophysical Research, 97, 6849-6866.

560 Jacobsen, S.D., Jiang, F., Mao, Z., Duffy, T.S., Smyth, J.R., Holl, C.M., and Frost, D.J. (2008)
561 Effects of hydration on the elastic properties of olivine. Geophysical Research Letters, 35,
562 L14303.

563 Jacobsen, S.D., and Smyth, J.R. (2006) Effect of water on the sound velocities of ringwoodite in
564 the transition zone. In: Jacobsen, S.D., van der Lee, S. (Eds.), Earth's deep water cycle.
565 American Geophysical Union, Washington, D.C., pp. 131-145.

566 Jacobsen, S.D., Smyth, J.R., Spetzler, H.A., Holl, C.M., and Frost, D.J. (2004) Sound velocities
567 and elastic constants of iron-bearing hydrous ringwoodite. Physics of the Earth and Planetary
568 Interiors, 143-144, 47-56.

569 Jordan, T.H. (1975) Lateral heterogeneity and mantle dynamics. Nature 257, 745-750.

570 Kantor, I., Prakapenka, V., Kantor, A., Dera, P., Kurnosov, A., Sinogeikin, S., Dubrovinskaia, N.,
571 and Dubrovinsky, L. (2012) BX90: A new diamond anvil cell design for X-ray diffraction and
572 optical measurements. Review of Scientific Instruments, 83, 125102.

573 Karato, S. (1995) Effects of water on seismic wave velocities in the upper mantle. Proceedings of
574 the Japan Academy, 71, 61-66.

575 Karato, S. (1998) Seismic anisotropy in the deep mantle, boundary layers and the geometry of
576 mantle convection. Pure and Applied Geophysics, 151, 565-587.

577 Karki, B.B., Stixrude, L., Clark, S.L., Warren, M.C., Ackland, G.J., and Crain, J. (1997) Structure
578 and elasticity of MgO at high pressure. American Mineralogist, 82, 51-60.

579 Katsura, T., Yoneda, A., Yamazaki, D., Yoshino, T., Ito, E. (2010) Adiabatic temperature profile
580 in the mantle. Physics of the Earth and Planetary Interiors, 183, 212-218.

581 Kimura, M., Sugiura, N., Mikouchi, T., Hirajima, T., Hiyagon, H., and Takehana, Y. (2013)
582 Eclogitic clasts with omphacite and pyrope-rich garnet in the NWA 801 CR2 chondrite.
583 American Mineralogist, 98, 387-393.

584 Lee, C.T.A. (2003) Compositional variation of density and seismic velocities in natural peridotites
585 at STP conditions: implications for seismic imaging of compositional heterogeneites in the
586 upper mantle. Journal of Geophysical Research, 108, B92441.

587 Leger, J.M., Redon, A.M., and Chateau, C. (1990) Compressions of synthetic pyrope, spessartine
588 and uvarovite garnets up to 25 GPa. Physics and Chemistry of Minerals, 17, 161-167.

589 Leitner, B.J., Weidner, D.J., Liebermann, R.C. (1980) Elasticity of single crystal pyrope and
590 implications for garnet solid solution series. Physics of the Earth and Planetary Interiors, 22,
591 111-121.

592 Levien, L., Prewitt, C.T., and Weidner, D.J. (1979) Compression of pyrope. American
593 Mineralogist, 64, 805-808.

594 Li, B.S., and Neuville, D.R. (2010) Elasticity of diopside to 8 GPa and 1073 K and implications
595 for the upper mantle. Physics of the Earth and Planetary Interiors, 183, 398-403.

596 Li, B.W., Ge, J.H., and Zhang, B.H. (2018) Diffusion in garnet: a review. Acta Geochimica, 37,
597 19-31.

598 Li, H.Y., Chen, R.X., Zheng, Y.F., and Hu, Z.C. (2018) Water in garnet pyroxenite from the Sulu
599 orogen: Implications for crust-mantle interaction in continental subduction zone. Chemical
600 Geology, 478, 18-38.

601 Li, L., Weidner, D.J., Brodholt, J., Alfè, D., and Price, G.D. (2011) Ab initio molecular dynamic
602 simulation on the elasticity of $Mg_3Al_2Si_3O_{12}$ pyrope. Journal of Earth Science, 22, 169-175.

603 Liu, L.G. (1980) The mineralogy of an eclogitic Earth mantle. Physics of the Earth and Planetary
604 Interiors, 23, 262-267.

605 Lu, R., and Keppler, H. (1997) Water solubility in pyrope to 100 kbar. Contributions to
606 Mineralogy and Petrology, 129, 35-42.

607 Lu, C., Mao, Z., Lin, J.F., Zhuravlev, K.K., Tkachev, S.N., and Prakapenka, V.B. (2013) Elasticity
608 of single-crystal iron-bearing pyrope up to 20 GPa and 750 K. Earth and Planetary Science
609 Letters, 361, 134-142.

610 Mao, H.K., Xu, J., and Bell, P.M. (1986) Calibration of the ruby pressure gauge to 800 kbar under
611 quasi-hydrostatic conditions. Journal of Geophysical Research, 91, 4673-4676.

612 Mao, Z., Fan, D.W., Lin, J.F., Yang, J., Tkachev, S.N., Zhuravlev, K., and Prakapenka, V.B.
613 (2015) Elasticity of single-crystal olivine at high pressures and temperatures. Earth and
614 Planetary Science Letters, 426, 204-215.

615 Mao, Z., Jacobsen, S.D., Frost, D.J., McCammon, C.A., Hauri, E.H., and Duffy, T.S. (2011)
616 Effect of hydration on the single-crystal elasticity of Fe-wadsleyite to 12 GPa. American
617 Mineralogist, 96, 1606-1612.

618 Mao, Z., Jacobsen, S.D., Jiang, F.M., Smyth, J.R., Holl, C.M., and Duffy, T.S. (2008) Elasticity of
619 hydrous wadsleyite to 12 GPa: implications for Earth's transition zone. Geophysical Research
620 Letters, 35, L21305.

621 Mao, Z., Jacobsen, S.D., Jiang, F.M., Smyth, J.R., Holl, C.M., Frost, D.J., and Duffy, T.S. (2010)
622 Velocity crossover between hydrous and anhydrous forsterite at high pressures. Earth and
623 Planetary Science Letters, 293, 250-258.

624 Mao, Z., Lin, J.F., Jacobsen, S.D., Duffy, T.S., Chang, Y.Y., Smyth, J.R., Frost, D.J., Hauri, E.H.,
625 and Prakapenka, V.B. (2012) Sound velocities of hydrous ringwoodite to 16 GPa and 673 K.
626 Earth and Planetary Science Letters, 331-332, 112-119.

627 McDonough, W.F., and Sun, S.S. (1995) The composition of the Earth. Chemical Geology, 120,
628 223-253.

629 Mookherjee, M., and Karato, S. (2010) Solubility of water in pyrope-rich garnet at high pressures
630 and temperature. Geophysical Research Letters, 37, L03310.

631 Murakami, M., Sinogeikin, S.V., Hellwig, H., Bass, J.D., and Li, J. (2007) Sound velocity of
632 $MgSiO_3$ perovskite to Mbar pressure. Earth and Planetary Science Letters, 256, 47-54.

633 Niu, F., Levander, A., Cooper, C.M., Lee, C.T.A., Lenardic, A., James, D.E. (2004) Seismic
634 constraints on the depth and composition of the mantle keel beneath the Kaapvaal craton. Earth
635 and Planetary Science Letters, 224, 337-346.

636 Nolet, G., Zielhuis, A. (1994) Low S velocities under the Tornquist-Teisseyre zone: evidence for
637 water injection into the transition zone by subduction. Geophysical Research Letters, 99,
638 15813-15820.

639 Ohtani, E. (2005) Water in the mantle. Elements, 1, 25-30.

640 Ohtani, E. (2015) Hydrous minerals and the storage of water in the deep mantle. Chemical
641 Geology, 418, 6-15.

642 O'Neill, B., Bass, J.D., Rossman, G.R., Geiger, C.A., and Langer, K. (1991) Elastic properties of
643 pyrope. Physics and Chemistry of Minerals, 17, 617-621.

644 Ostwald, J., Pazold, W., and Weis, O. (1977) High-resolution Brillouin spectroscopy of water.
645 Applied Physics, 13, 351-356.

646 Poli, S., and Schmidt, M.W. (2002) Petrology of subducted slabs. Annual Review of Earth and
647 Planetary Sciences, 30, 207-235.

648 Polian, A., Vo-Thanh, D., and Richet, P. (2002) Elastic properties of α-SiO_2 up to 2300 K from
649 Brillouin scattering measurements. Europhysics Letters, 57, 375-381.

650 Rickwood, P.C., Mathias, M., Siebert, J.C. (1968) A study of garnets from eclogite and peridotite
651 xenoliths found in kimberlite. Contributions to Mineralogy and Petrology, 19, 271-301.

652 Ringwood, A.E. (1975) Composition and petrology of the Earth's mantle. McGraw-Hill, New
653 York.

654 Ringwood, A.E. (1982) Phase transformations and differentiation in subducted lithosphere:
655 implications for mantle dynamics, basalt petrogenesis, and crustal evolution. The Journal of
656 Geology, 90, 611-643.

657 Ringwood, A.E. (1991) Phase transformations and their bearing on the constitution and dynamics
658 of the mantle. Geochimica et Cosmochimica Acta, 55, 2083-2110.

659 Rivers, M., Prakapenka, V.B., Kubo, A., Pullins, C., Holl, C.M., and Jacobsen, S.D. (2008) The
660 COMPRES/GSECARS gas-loading system for diamond anvil cells at the Advanced Photon
661 Source. High Pressure Research, 28, 273-292.

662 Rossman, G.R., Beran, A., and Langer, K. (1989) The hydrous component of pyrope from the
663 Dora Maira Massif, Western Alps. Physics and Chemistry of Minerals, 1, 151-154.

664 Sang, L.Q., and Bass, J.D. (2014) Single-crystal elasticity of diopside to 14 GPa by Brillouin
665 scattering. Physics of the Earth and Planetary Interiors, 228, 75-79.

666 Sato, Y., Akaogi, M., and Akimoto, S. (1978) Hydrostatic compression of the synthetic garnets
667 pyrope and almandine. Journal of Geophysical Research, 83, 335-338.

668 Sinogeikin, S.V., and Bass, J.D. (2000) Single-crystal elasticity of pyrope and MgO to 20 GPa by
669 Brillouin scattering in the diamond cell. Physics of the Earth and Planetary Interiors, 120,
670 43-62.

671 Sinogeikin, S.V., and Bass, J.D. (2002) Elasticity of pyrope and majorite-pyrope solid solutions to
672 high temperatures. Earth and Planetary Science Letters, 203, 549-555.

673 Sinogeikin, S.V., Bass, J.D., and Katsura, T. (2003) Single-crystal elasticity of ringwoodite to
674 high pressures and high temperatures: implications for 520 km seismic discontinuity. Physics of
675 the Earth and Planetary Interiors, 136, 41-66.

676 Sinogeikin, S.V., Bass, J.D., Prakapenka, V., Lakshtanov, D., Shen, G., Sanchez-Valle, C., and
677 Rivers, M. (2006) Brillouin spectrometer interfaced with synchrotron radiation for simultaneous
678 X-ray density and acoustic velocity measurements. Review of Scientific Instruments, 77,
679 103905.

680 Skogby, H. (2006) Water in natural mantle minerals I: Pyroxenes. Reviews in Mineralogy and
681 Geochemistry, 62, 155-167.

682 Smyth, J.R. (1987) β-Mg_2SiO_4: A potential host for water in the mantle? American Mineralogist,
683 72, 1051-1055.

684 Smyth, J.R., Holl, C.M., Frost, D.J., Jacobsen, S.D., Langenhorst, F., McCammon, C.A. (2003)
685 Structural systematics of hydrous ringwoodite and water in Earth's interior. American
686 Mineralogist, 88, 1402-1407.

687 Smyth, J.R. and Jacobsen, S.D. (2006) Nominally anhydrous minerals and Earth's deep water
688 cycle. In Jacobsen, S.D., and van der Lee, S. (Eds.) Earth's Deep Water Cycle. Geophysical
689 Monograph Series, vol. 168, pp. 1-11, American Geophysical Union, Washington, D.C.

690 Song, T.A., Helmberger, D.V., and Grand, S.P. (2004) Low-velocity zone atop the 410-km
691 seismic discontinuity in the northwestern United States. Nature, 427, 530-533.

692 Speziale, S., Jiang, F., and Duffy, T.S. (2005) Compositional dependence of the elastic wave
693 velocities of mantle minerals: implications for seismic properties of mantle rocks. In: van der

694 Hilst, et al. (Eds.) Earth's deep mantle: structure, composition, and evolution. Geophysical
695 Monograph Series, vol. 160, pp. 301-320, American Geophysical Union, Washington, D.C.

696 Speziale, S. Marquardt, H., Duffy, T.S. (2014) Brillouin Scattering and its Application in
697 Geosciences. Reviews in Mineralogy & Geochemistry, 78, 543-603.

698 Sumino, Y., and Nishizawa, O. (1978) Temperature variation of elastic constants of
699 pyrope-almandine garnets. Journal of Physics of the Earth, 26, 239-252.

700 Suzuki, I., and Anderson, O.L. (1983) Elasticity and thermal expansion of a natural garnet up to
701 1000 K. Journal of Physics of the Earth, 31, 125-138.

702 Thieblot, L., Roux, J., Richet, P. (1998) High-temperature thermal expansion and decompositions
703 of garnets. European Journal of Mineralogy, 10, 7-15.

704 van der Meijde, M., Marone, F., Giardini, D., van der Lee, S. (2003) Seismic evidence for water
705 deep in Earth's upper mantle. Science, 300, 1556-1558.

706 Wang, J., Sinogeikin, S.V., Inoue, T., and Bass, J.D. (2003) Elastic properties of hydrous
707 ringwoodite. American Mineralogist, 88, 1608-1611.

708 Wang, J., Sinogeikin, S.V., Inoue, T., and Bass, J.D. (2006) Elastic properties of hydrous
709 ringwoodite at high-pressure conditions. Geophysical Research Letters, 33, L14308.

710 Wang, Y., Weidner, D.J., Zhang, J., Gwanrnesia, G.D., Liebermann, R.C., and Bass, J.D. (1998)
711 Thermal equation of state of garnets along the pyrope-majorite join. Physics of the Earth and
712 Planetary Interiors, 105, 59-71.

713 Weidner, D.J., and Wang, Y. (2000) Phase transformations: implications for mantle structure. In:
714 Karato, S.I. et al. (Eds.) Earth's Deep Interior: Mineral Physics and Tomography From the
715 Atomic to the Global Scale. Geophysical Monograph Series, vol. 117. pp. 215-235, American
716 Geophysical Union, Washington, D.C.

717 Withers, A.C., Wood, B.J., and Carroll, M.R. (1998) The OH content of pyrope at high pressure.
718 Chemical Geology, 147, 161-171.

719 Xu, J.G., Zhang, D.Z., Fan, D.W., Dera, P., Shi, F., and Zhou, W.G. (2019) Thermoelastic
720 properties of eclogitic ternary garnets and omphacites: Implications for deep subduction of
721 oceanic crust and density anomalies in the upper mantle. Geophysical Research Letters, 46,
722 179-188.

723 Yang, J., Lin, J.F., Jacobsen, S.D., Seymour, N.M., Tkachev, S.N., and Prakapenka, V.B. (2016)
724 Elasticity of ferropericlase and seismic heterogeneity in the Earth's lower mantle. Journal of
725 Geophysical Research, 121, 8488-8500.

726 Yang, J., Mao, Z., Lin, J.F., and Prakapenka, V.B. (2014) Single-crystal elasticity of the
727 deep-mantle magnesite at high pressure and temperature. Earth and Planetary Science Letters,
728 392, 292-299.

729 Yang, J., Tong, X.Y., Lin, J.F., Okuchi, T., and Tomioka, N. (2015) Elasticity of ferropericlase
730 across the spin crossover in the Earth's lower mantle. Scientific Reports, 5, 17188.

731 Ye, Y., Smyth, J.R., Hushur, A., Manghnani, M.H., Lonappan, D., Dera, P., Frost, D.J. (2010)
732 Crystal structure of hydrous wadsleyite with 2.8% H_2O and compressibility to 60 GPa.
733 American Mineralogist, 95, 1765-1772.

734 Ye, Y., Brown, D.A., Smyth, J.R., Panero, W.R., Jacobsen, S.D., Chang, Y.Y., Townsend, J.P.,
735 Thomas, S.M., Hauri, E.H., Dera, P., Frost, D.J. (2012) Compressibility and thermal expansion
736 of hydrous ringwoodite with 2.5(3) wt% H_2O. American Mineralogist, 97, 573-582.

737 Zha, C.S., Duffy, T.S., Downs, R.T., Mao, H.K., Hemley, R.J. (1996) Sound velocity and
738 elasticity of single-crystal forsterite to 16 GPa. Journal of Geophysical Research, 101,
739 17535-17545.

740 Zhang, J.S. and Bass, J.D. (2016) Single-crystal elasticity of natural Fe-bearing orthoenstatite
741 across a high-pressure phase transition. Geophysical Research Letters, 43, 8473-8481.

742 Zhang, L., Ahsbahs, H., and Kutoglu, A. (1998) Hydrostatic compression and crystal structure of
743 pyrope to 33 GPa. Physics and Chemistry of Minerals, 25, 301-307.

744 Zou, Y.T., Gréaux, S., Irifune, T., Whitaker, M.L., Shinmei, T., and Higo, Y. (2012a) Thermal
745 equation of state of $Mg_3Al_2Si_3O_{12}$ pyrope garnet up to 19 GPa and 1,700 K. Physics and
746 Chemistry of Minerals, 39, 589-598.

747 Zou, Y.T., Irifune, T., Gréaux, S., Whitaker, M.L., Shinmei, T., Ohfuji, H., Negishi, R., and Higo,
748 Y. (2012b) Elasticity and sound velocities of polycrystalline $Mg_3Al_2(SiO_4)_3$ garnet up to 20GPa
749 and 1700K. Journal of Applied Physics, 112, 014910.

750 **Figure Captions**

751 **Figure 1.** Representative Brillouin spectra of single-crystal hydrous pyrope at 18.6
752 GPa and 300 K (a), and 1 atm and 700 K (b). Open circles: experimental data; solid
753 lines: fitted V_P and V_S peaks, respectively. The average collection time was ~ 40 min
754 and ~ 20 min for each spectrum of high-pressure and high-temperature measurements,
755 respectively. The (0.34, -0.53, 0.92) crystallographic plane of single-crystal hydrous
756 pyrope sample was used for both BLS experiments. Experimental uncertainties are
757 smaller than the symbols. (Color online.)
758
759 **Figure 2.** V_P and V_S velocities of single-crystal hydrous pyrope as a function of the
760 azimuthal angel measured at 18.6 GPa and 300 K (a), and 1 atm and 700 K (b). Open
761 circles: experimental data; solid lines: modeled results. Error bars are smaller than the
762 symbols when not shown. (Color online.)
763
764 **Figure 3.** Single-crystal individual elastic moduli (C_{11}, C_{12}, and C_{44}) of hydrous
765 pyrope as a function of pressure (a) and temperature (b) compared with previous
766 study of anhydrous pyrope. Solid symbols represent our experimental data; solid lines
767 are modeled results using the third-order finite-strain equation fitting (a) or a linear
768 fitting (b); dashed lines represent the experimental data of anhydrous pyrope
769 (Sinogeikin and Bass 2000, 2002). Error bars are smaller than the symbols when not
770 shown. (Color online.)
771

Figure 4. Adiabatic bulk (K_S) and shear modulus (G) of hydrous pyrope as a function of pressure (a) and temperature (b) compared with previous study of anhydrous pyrope. Solid symbols represent our experimental data; solid lines are modeled results using the third-order finite-strain equation fitting (a) or a linear fitting (b); dashed lines represent the experimental data of anhydrous pyrope (Sinogeikin and Bass 2000, 2002). Error bars are smaller than the symbols when not shown. (Color online.)

Figure 5. Aggregate compressional (V_P) and shear velocity (V_S) of hydrous pyrope as a function of pressure (a) and temperature (b) compared with previous study of anhydrous pyrope. Solid symbols represent our experimental data; solid lines are modeled results using the third-order finite-strain equation fitting (a) or a linear fitting (b); dashed lines represent the experimental data of anhydrous pyrope (Sinogeikin and Bass 2000, 2002). Error bars are smaller than the symbols when not shown. (Color online.)

Figure 6. Modeled velocities of pyrope garnets in the Earth's upper mantle along the upper mantle geotherm and cold subducted slabs geotherm. Red lines: hydrous pyrope (this study; Fan et al. 2017b); blue lines: anhydrous pyrope (Sinogeikin and Bass, 2000, 2002; Zou et al. 2012a); black lines: (Fe,Ca)-bearing pyrope (Lu et al. 2013; Thieblot et al. 1998). Error bars represent the propagated uncertainties (±1σ). (Color online.)

Figure 7. Comparison of modeled V_P/V_S ratio of hydrous pyrope with anhydrous pyrope and (Fe,Ca)-bearing pyrope in the Earth's upper mantle along the upper mantle geotherm and cold subducted slabs geotherm. Error bars represent the propagated uncertainties (±1σ). (Color online.)

This is a preprint, the final version is subject to change, of the American Mineralogist (MSA)
Cite as Authors (Year) Title. American Mineralogist, in press.
DOI: https://doi.org/10.2138/am-2019-6897

Table 1 Densities, elastic moduli and aggregate velocities of hydrous pyrope at high pressure and ambient temperature

P (GPa)	Density (g/cm^3)	C_{11} (GPa)	C_{12} (GPa)	C_{44} (GPa)	K_V (GPa)	K_R (GPa)	K_S (GPa)	G_V (GPa)	G_R (GPa)	G (GPa)	V_P (km/s)	V_S (km/s)	V_P/V_S	AV
0.0001	3.557(2)	294.5(5)	105.7(6)	90.5(4)	168.6(4)	168.6(4)	168.6(4)	92.1(2)	92.0(3)	92.0(3)	9.05(1)	5.09(1)	1.78(1)	-0.026(1)
0.9(1)	3.577(2)	301.7(5)	109.9(6)	91.4(4)	173.8(3)	173.8(3)	173.8(3)	93.1(2)	93.2(3)	93.2(3)	9.13(1)	5.10(1)	1.79(1)	-0.030(1)
3.4(2)	3.629(3)	316.8(6)	119.2(7)	94.3(5)	185.1(4)	185.1(4)	185.1(4)	96.0(2)	96.1(2)	96.1(2)	9.29(1)	5.15(1)	1.81(1)	-0.028(1)
5.8(2)	3.677(3)	331.6(6)	126.3(5)	97.7(4)	194.7(5)	194.7(5)	194.7(5)	99.6(2)	99.7(2)	99.7(2)	9.44(1)	5.21(1)	1.81(1)	-0.030(1)
7.5(1)	3.709(2)	339.7(7)	133.5(6)	100.6(5)	202.2(4)	202.2(4)	202.2(4)	101.6(2)	101.6(2)	101.6(2)	9.54(1)	5.23(1)	1.82(1)	-0.015(1)
10.1(2)	3.757(2)	355.2(7)	142.6(7)	103.5(5)	213.5(3)	213.5(3)	213.5(3)	104.6(2)	104.6(3)	104.6(3)	9.69(1)	5.28(1)	1.84(1)	-0.016(1)
12.3(2)	3.795(3)	368.5(8)	150.6(7)	106.8(5)	223.2(3)	223.2(3)	223.2(3)	107.6(1)	107.7(2)	107.7(2)	9.83(1)	5.33(1)	1.85(1)	-0.012(1)
15.5(3)	3.849(3)	387.4(7)	162.5(6)	110.7(6)	237.5(4)	237.5(4)	237.5(4)	111.4(2)	111.4(2)	111.4(2)	10.01(1)	5.38(1)	1.86(1)	-0.009(1)
18.6(2)	3.899(3)	404.6(8)	174.8(8)	115.2(6)	251.4(5)	251.4(5)	251.4(5)	115.1(1)	115.1(2)	115.1(2)	10.19(1)	5.43(1)	1.88(1)	0.0010(2)

Numbers in parenthesis represent standard deviations.

This is a preprint, the final version is subject to change, of the American Mineralogist (MSA)
Cite as Authors (Year) Title. American Mineralogist, in press.
DOI: https://doi.org/10.2138/am-2019-6897

Table 2 Densities, elastic moduli and aggregate velocities of hydrous pyrope at ambient pressure and high temperature

T (K)	Density (g/cm^3)	C_{11} (GPa)	C_{12} (GPa)	C_{44} (GPa)	K_V (GPa)	K_R (GPa)	K_S (GPa)	G_V (GPa)	G_R (GPa)	G (GPa)	V_P (km/s)	V_S (km/s)	V_P/V_S	AV
300[a]	3.557(3)	294.8(6)	105.5(4)	90.7(5)	168.6(5)	168.6(5)	168.6(5)	92.2(3)	92.3(4)	92.3(4)	9.05(1)	5.09(1)	1.78(1)	-0.027(1)
300	3.557(2)	294.5(5)	105.7(6)	90.5(4)	168.6(4)	168.6(4)	168.6(4)	92.0(2)	92.1(3)	92.0(3)	9.05(1)	5.09(1)	1.78(1)	-0.026(1)
400	3.546(3)	291.8(4)	104.9(4)	89.9(2)	167.2(3)	167.2(3)	167.2(3)	91.3(2)	91.3(2)	91.3(2)	9.03(1)	5.07(1)	1.78(1)	-0.024(1)
500	3.534(2)	289.1(5)	104.1(6)	89.3(3)	165.8(3)	165.8(3)	165.8(3)	90.6(1)	90.6(2)	90.6(2)	9.00(1)	5.06(1)	1.78(1)	-0.022(1)
600	3.523(3)	286.6(5)	103.2(5)	88.7(4)	164.3(3)	164.3(3)	164.3(3)	89.9(2)	89.9(2)	89.9(2)	8.98(1)	5.05(1)	1.78(1)	-0.021(1)
700	3.511(3)	283.4(5)	102.3(6)	87.9(4)	162.7(4)	162.7(4)	162.7(4)	89.0(2)	89.0(3)	89.0(3)	8.95(1)	5.03(1)	1.78(1)	-0.019(1)

Numbers in parenthesis represent standard deviations.

[a)] Represents measurement at temperature decreased from 700 K to room temperature.

This is a preprint, the final version is subject to change, of the American Mineralogist (MSA)
Cite as Authors (Year) Title. American Mineralogist, in press.
DOI: https://doi.org/10.2138/am-2019-6897

Table 3 Single-crystal elastic moduli and their pressure and temperature derivatives of hydrous pyrope at ambient conditions in comparison to previous studies [a]

References	Composition	Method	C_{11} (GPa)	C_{12} (GPa)	C_{44} (GPa)	$(\partial C_{11}/\partial P)_T$	$(\partial C_{12}/\partial P)_T$	$(\partial C_{44}/\partial P)_T$	$(\partial C_{11}/\partial T)_P$ (GPa/K)	$(\partial C_{12}/\partial T)_P$ (GPa/K)	$(\partial C_{44}/\partial T)_P$ (GPa/K)
This study	Hydrous Prp100 [c]	BLS	294.5(5)	105.7(6)	90.5(4)	6.2(1)	3.7(1)	1.5(1)	-0.028(1)	-0.009(1)	-0.006(1)
O'Neill et al. (1991)	Hydrous Prp100 [d]	BLS	296.2(5)	111.1(6)	91.6(3)	—[b]	—[b]	—[b]	—[b]	—[b]	—[b]
Leitner et al. (1980)	Prp100	BLS	295(2)	117(1)	90(3)	—[b]	—[b]	—[b]	—[b]	—[b]	—[b]
Sinogeikin and Bass (2000)	Prp100	BLS	297(3)	108(2)	93(2)	5.8(4)	3.2(4)	1.3(3)	—[b]	—[b]	—[b]
Sinogeikin and Bass (2002)	Prp100	BLS	298(3)	107(2)	93(2)	—[b]	—[b]	—[b]	-0.031(3)	-0.006(2)	-0.007(2)
Lu et al. (2013)	Prp68Alm24Grs5	BLS	290(2)	106(2)	92.2(6)	6.0(1)	3.5(1)	1.2(1)	-0.021(4)	-0.0163(5)	-0.003(1)

Numbers in parenthesis represent standard deviations. Prp: Pyrope; Alm: Almandine; Grs: Grossular; BLS: Brillouin Light Scattering.

[a] Only Brillouin scattering results are listed for pyrope garnet.

[b] The value is not available in the text.

[c] ~900 ppmw H_2O.

[d] ~180 ppmw H_2O.

This is a preprint, the final version is subject to change, of the American Mineralogist (MSA)
Cite as Authors (Year) Title. American Mineralogist, in press.
DOI: https://doi.org/10.2138/am-2019-6897

Table 4 Bulk and shear moduli and their pressure and temperature derivatives of hydrous pyrope at ambient conditions in comparison to previous studies [a]

References	Composition	Methods	K_{S0} (GPa)	G_0 (GPa)	$(\partial K_S/\partial P)_T$	$(\partial G/\partial P)_T$	$(\partial K_S/\partial T)_P$ (GPa/K)	$(\partial G/\partial T)_P$ (GPa/K)
This study	Hydrous Prp100	BLS	168.6(4)	92.0(3)	4.6(1)	1.3(1)	-0.015(1)	-0.008(1)
O'Neill et al. (1991)	Hydrous Prp100	BLS	172.8(3)	92.0(2)	—[b]	—[b]	—[b]	—[b]
Leitner et al. (1980)	Prp100	BLS	177(1)	89(1)	—[b]	—[b]	—[b]	—[b]
Conrad et al. (2000)	Prp100	BLS	172.7[c]	92[c]	3.2[c]	1.4[c]	—[b]	—[b]
Sinogeikin and Bass (2000)	Prp100	BLS	171(2)	94(2)	4.1(3)	1.3(2)	—[b]	—[b]
Sinogeikin and Bass (2002)	Prp100	BLS	171(2)	94(2)	—[b]	—[b]	-0.014(2)	-0.009(1)
Lu et al. (2013)	Prp68Alm24Grs5	BLS	168(2)	92(1)	4.4(1)	1.2(1)	-0.017(1)	-0.005(1)
Chen et al. (1999)	Prp100	UI	171(20)	92(1)	5.3(4)	1.6(2)	—[b]	—[b]
Gwanmesia et al. (2006)	Prp100	UI	175(2)	91(1)	3.9(3)	1.7(2)	-0.018(2)	-0.010(1)
Zou et al. (2012)	Prp100	UI	170.0(2)	93.2(1)	4.51(2)	1.51(2)	-0.0170(1)	-0.0107(1)
Chantel et al. (2016)	Prp100	UI	172(2)	89.1(5)	4.38(8)	1.66(5)	-0.018(2)	-0.008(1)

Numbers in parenthesis represent standard deviations.

[a] Only Brillouin scattering and ultrasonic interferometry results are listed for pyrope garnet.

[b] The value is not available in the text.

[c] The uncertainty is not available in the text.

This is a preprint, the final version is subject to change, of the American Mineralogist (MSA)
Cite as Authors (Year) Title. American Mineralogist, in press.
DOI: https://doi.org/10.2138/am-2019-6897

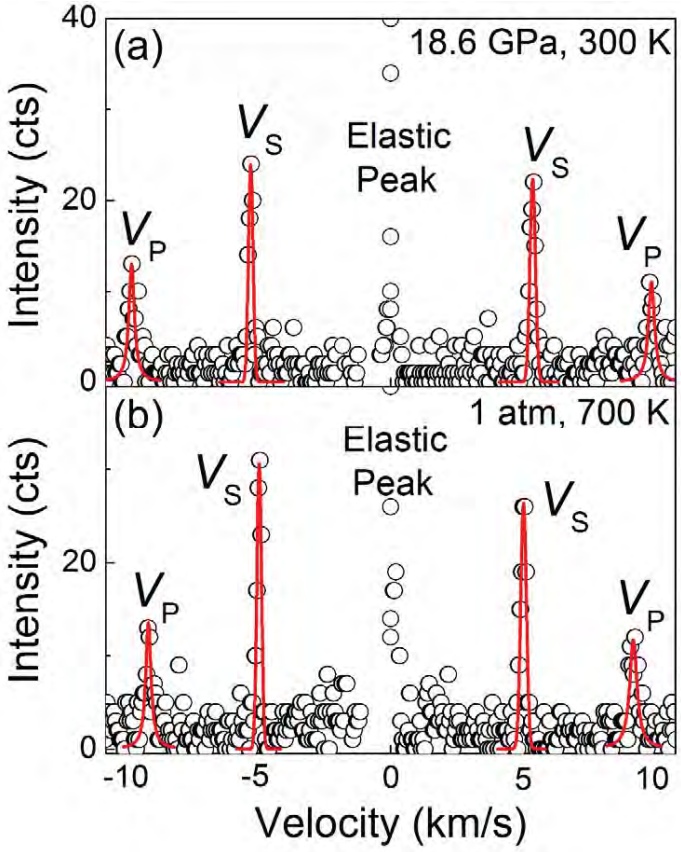

Fig. 1

This is a preprint, the final version is subject to change, of the American Mineralogist (MSA)
Cite as Authors (Year) Title. American Mineralogist, in press.
DOI: https://doi.org/10.2138/am-2019-6897

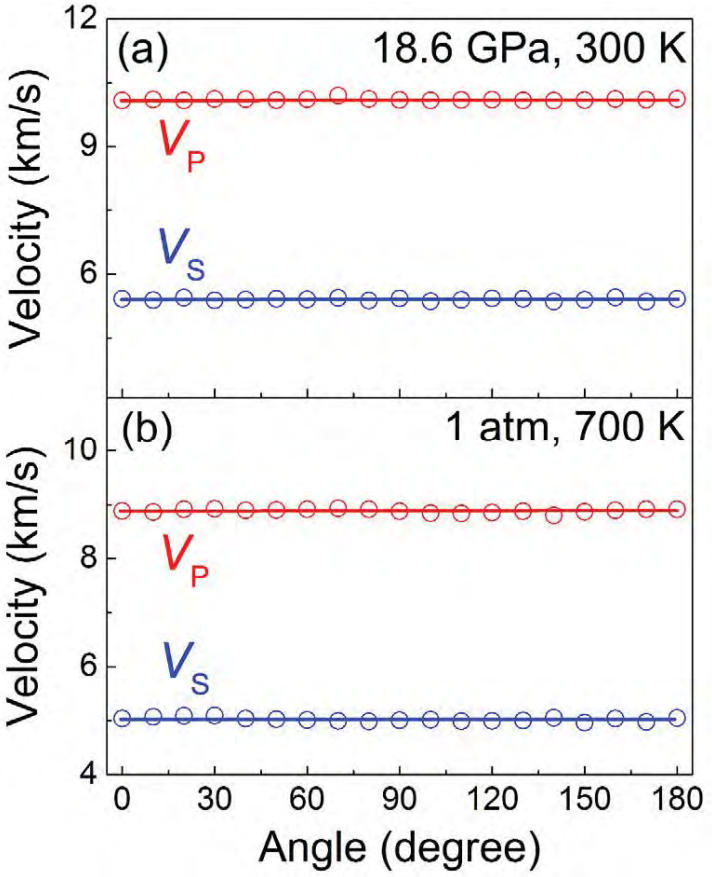

Fig. 2

This is a preprint, the final version is subject to change, of the American Mineralogist (MSA)
Cite as Authors (Year) Title. American Mineralogist, in press.
DOI: https://doi.org/10.2138/am-2019-6897

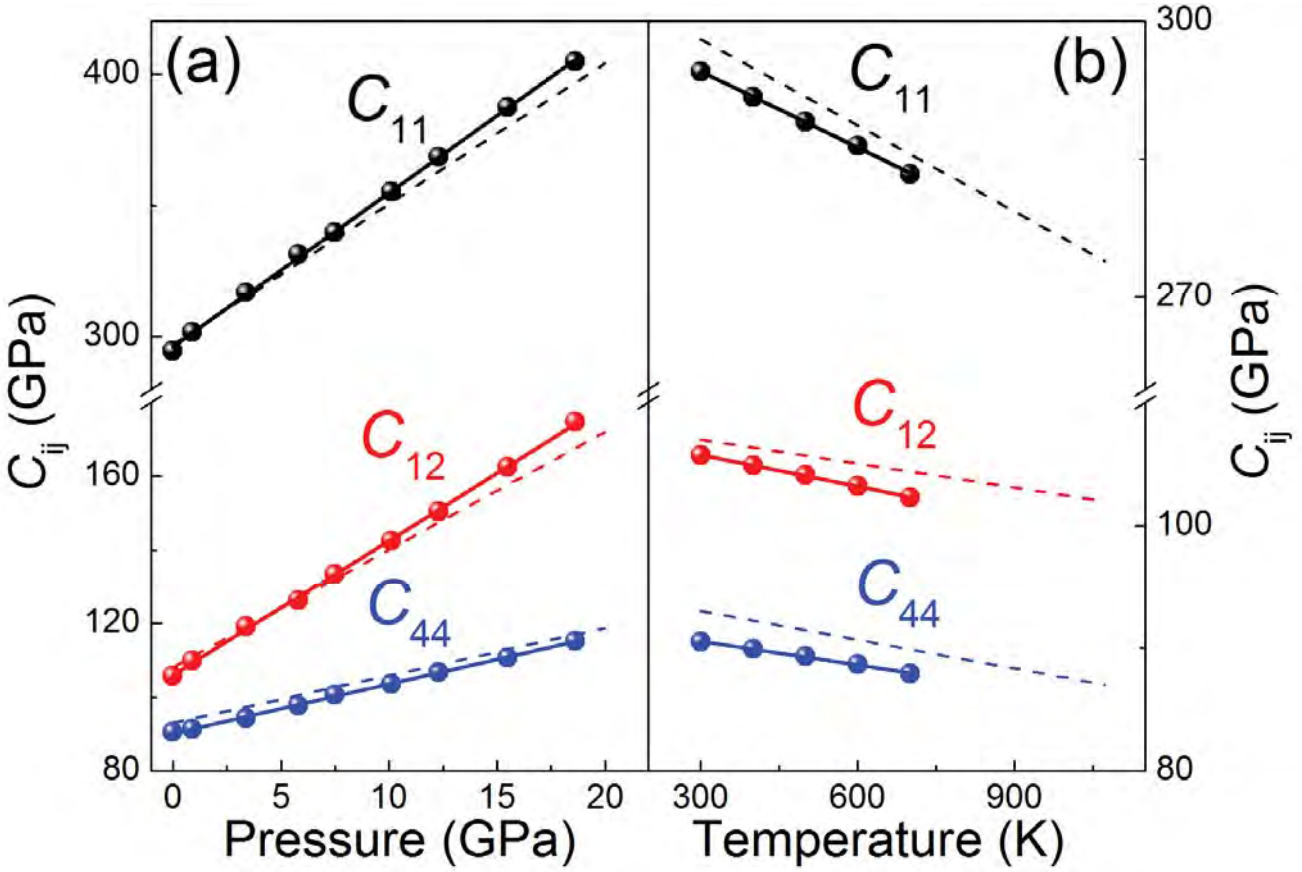

Fig. 3

This is a preprint, the final version is subject to change, of the American Mineralogist (MSA)
Cite as Authors (Year) Title. American Mineralogist, in press.
DOI: https://doi.org/10.2138/am-2019-6897

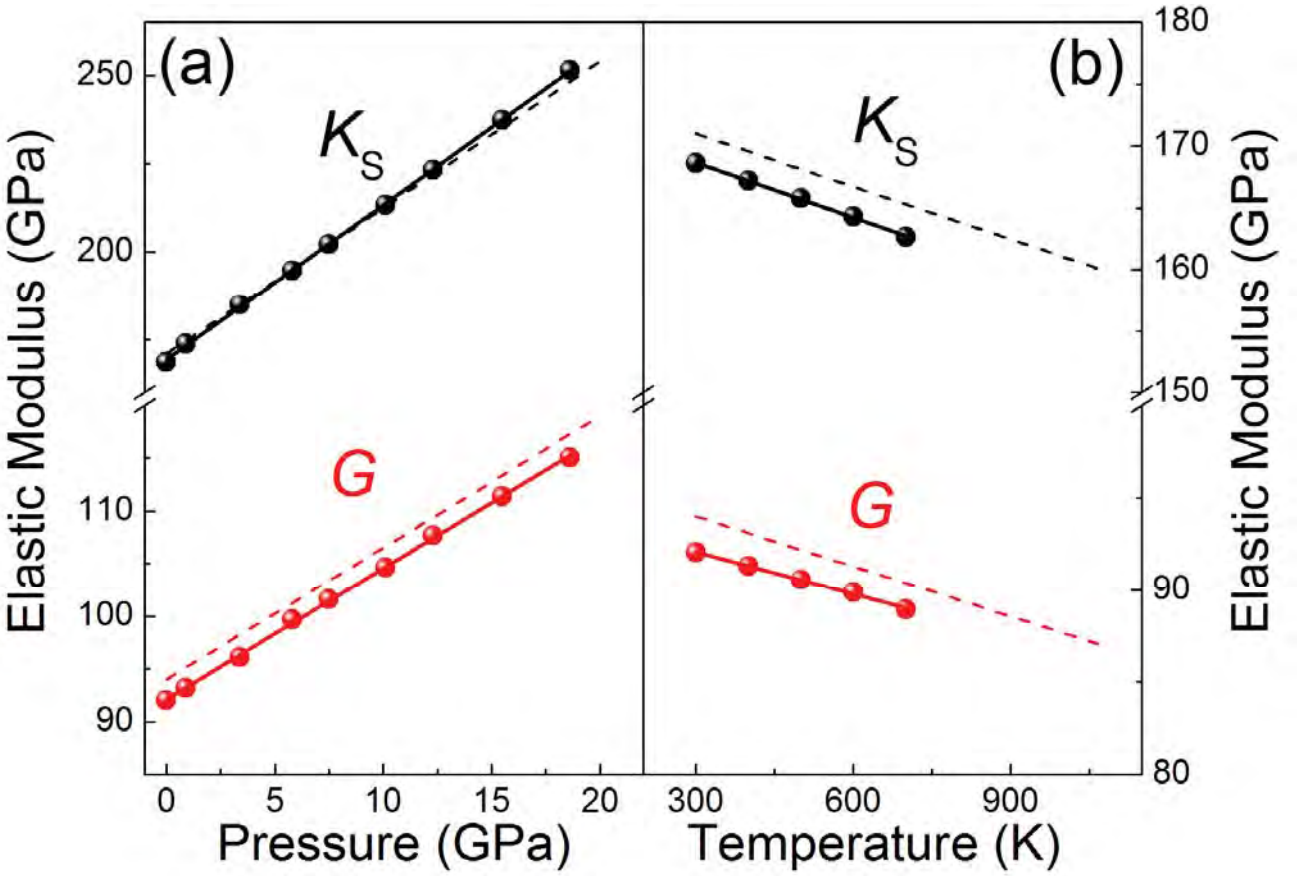

Fig. 4

This is a preprint, the final version is subject to change, of the American Mineralogist (MSA)
Cite as Authors (Year) Title. American Mineralogist, in press.
DOI: https://doi.org/10.2138/am-2019-6897

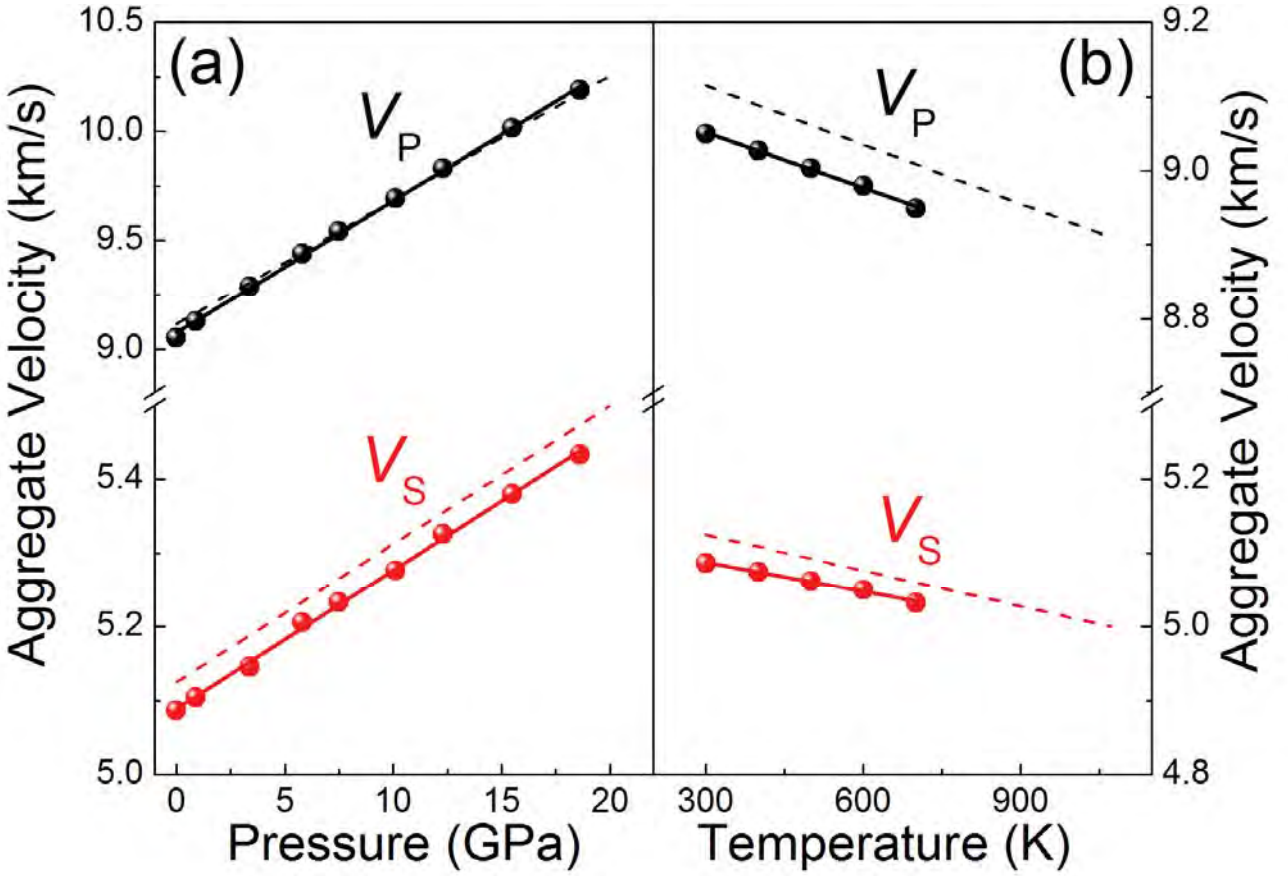

Fig. 5

This is a preprint, the final version is subject to change, of the American Mineralogist (MSA)
Cite as Authors (Year) Title. American Mineralogist, in press.
DOI: https://doi.org/10.2138/am-2019-6897

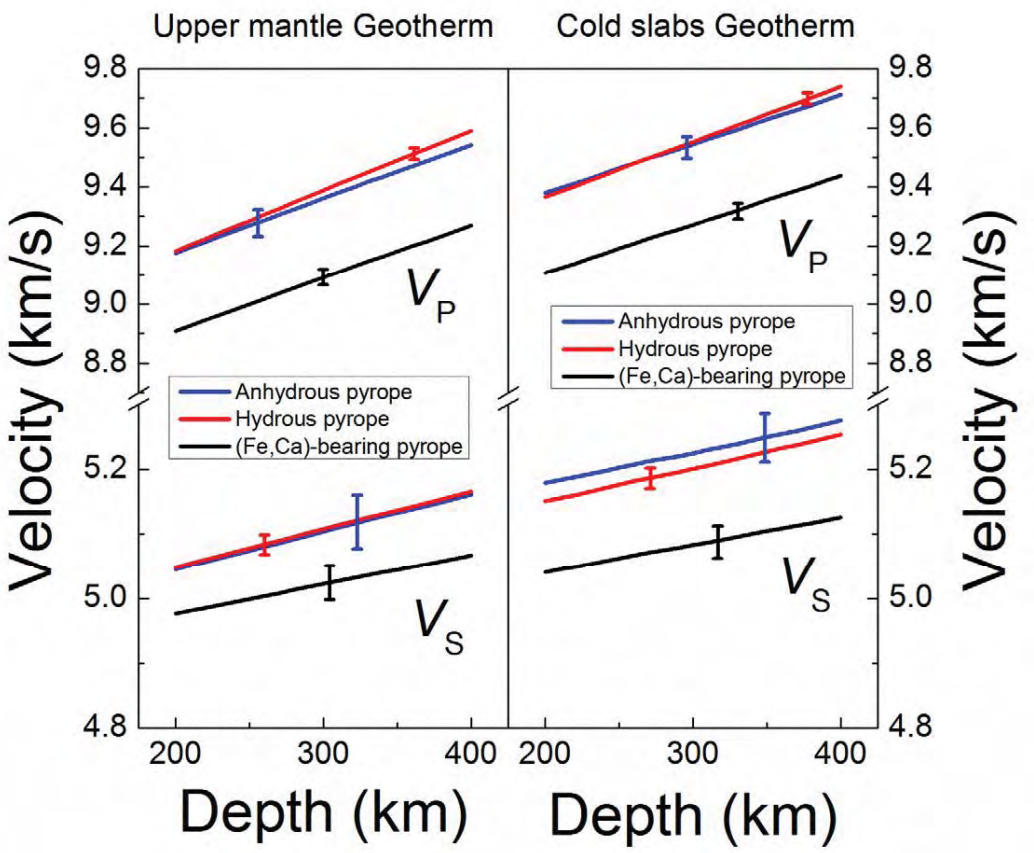

Fig. 6

This is a preprint, the final version is subject to change, of the American Mineralogist (MSA)
Cite as Authors (Year) Title. American Mineralogist, in press.
DOI: https://doi.org/10.2138/am-2019-6897

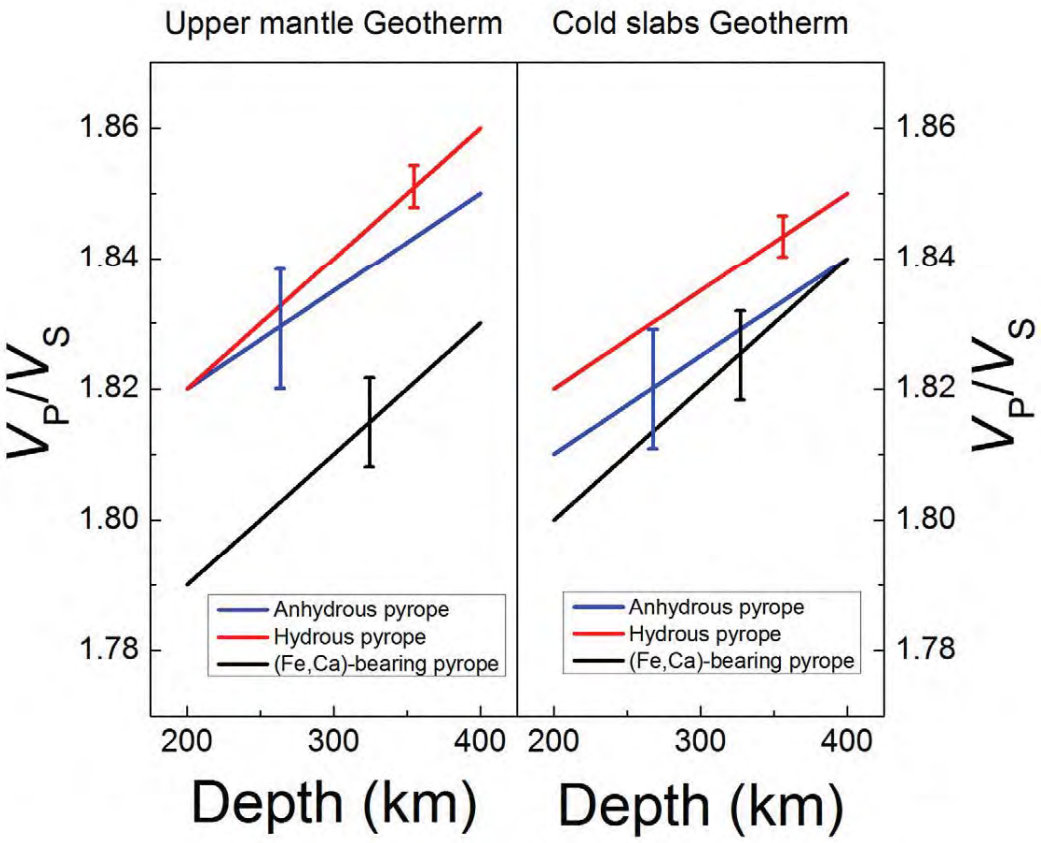

Fig. 7